Semiclassical cross section for a classically chaotic scattering system

1990 J. Phys. A: Math. Gen. 23 3729

(http://iopscience.iop.org/0305-4470/23/16/021)

J. Phys. A: Math. Gen. 23 (1990) 3729–3748. Printed in the UK

Semiclassical cross section for a classically chaotic scattering system

C Jung and S Pott
Fachbereich Physik, Universität Bremen, 2800 Bremen, Federal Republic of Germany

Received 9 February 1990

Abstract. A semiclassical treatment of the scattering cross section of a classically chaotic scattering problem is presented. In the limit of small $\hbar$ we find several ways in which images of classical fractal structures show up in the semiclassical cross section. First, the fractal arrangement of rainbow singularities emerges. Further, the interference terms in the semiclassical cross section show oscillations on all scales, whose frequency spectra approach fractal structures which are well known from the classical system. This holds for the cross section as a function of the scattering angle for fixed energy as well as for the cross section as a function of energy for fixed scattering angle.

1. Introduction

The phenomenon of chaotic classical scattering has been known for some time and was studied most extensively in classical models for inelastic molecular scattering [1–9]. Chaotic scattering of the same type has also been found in satellite encounters [10], in an inclined billiard [11], in vortex motion in hydrodynamics [12], in soliton scattering [13] and in elastic potential scattering [14–18]. See also the review articles [19, 20] and references therein.

In all these systems the final asymptote has been observed as function of the initial asymptote and this function displays discontinuities on a fractal subset of its domain. The explanation is as follows. By homoclinic and heteroclinic connections of unstable periodic orbits a hyperbolic invariant set Λ in the phase space is created. The stable manifolds of the infinitely many localized orbits reach out into the incoming asymptotic region and cause a subset of incoming scattering trajectories with measure zero to get stuck inside the potential region. The other generic scattering trajectories with proper incoming and outgoing asymptotes are not chaotic themselves. However, they flow through the gaps of Λ and project some kind of shadow image of the chaotic set Λ into the outgoing asymptotic region. By measurements of the mapping from incoming to outgoing asymptotes many properties of the localized chaos can be recovered. Scattering trajectories coming close to Λ spend a long time inside the potential interior and run long distances alongside localized orbits. Accordingly, scattering chaos can be treated as a kind of transient chaos [21, 22].

The phenomena just described are possible within classical dynamics only. However, scattering experiments are an important source of information for micro systems, where quantum effects are essential. It is therefore important to find the quantum mechanical phenomena which correspond to irregular scattering in classical mechanics.

0305-4470/90/163729+20$03.50

So far, not much has been done for the investigation of quantum irregular scattering. There is an investigation of the phase shift in the quantum mechanical scattering amplitude for a solvable model [23]. The scattering phase could be expressed by a Riemann ζ function, which represents a chaotic function. An explanation of the statistical properties of the fast fluctuations of the cross section as a function of the energy has been given within a semiclassical approximation [24–26]. These results explain the behaviour which comes out of random matrix models which have been used to describe the fast fluctuations in the cross section found in nuclear scattering. A semiclassical treatment of the resonance poles for chaotic scattering systems is presented in [27]. A comparison of the quantum mechanical behaviour with the classical and semiclassical behaviour is given for two different model systems in [25] and in [18].

Because the scattering cross section is the most important observable quantity in scattering systems, in this paper we try to find fingerprints of the classical chaos in the semiclassical differential cross section. For simplicity we treat the scattering of a mass point moving in a two-dimensional position space under the influence of a local potential. For most of our discussions we use the particular potential of equation (1) and make a few remarks on the generality of our considerations later.

$$V(x,y) = \exp[-(x+\sqrt{2})^2 - y^2] + \exp[-(x-1/\sqrt{2})^2 - (y+\sqrt{3/2})^2] + \exp[-(x-1/\sqrt{2})^2 - (y-\sqrt{3/2})^2] \tag{1}$$

where x, y are Cartesian coordinates in position space. The system is invariant under rotations by $\pm 2\pi/3$. V has seven critical points: a relative minimum in the origin $P_0 = (0,0)$ at energy $E_0 = 0.40...$; three saddles P_{S1}, P_{S2}, P_{S3} at energy $E_S = 0.45...$; and three maxima P_{M1}, P_{M2}, P_{M3} at energy $E_M = 1.005$. The set of saddle points $\{P_S i,\ i = 1,2,3\}$ and the set of maxima $\{P_{Mi},\ i = 1,2,3\}$ are invariant under rotations through $+2\pi/3$ and $-2\pi/3$ around the origin $P_{S1} = (0.6...,0)$, $P_{M1} = (-1.4...,0)$.

System (1) has a remarkable property: there is an energy value $E_B \approx 0.483$ such that for each energy value $E \in [E_B, E_M]$ the exact symbolic dynamics of the hyperbolic set Λ can be given in closed form. System (1) has C_{3v} symmetry and in the symmetry-reduced phase space there is exactly one localized orbit belonging to Λ for each infinite binary symbolic sequence. Periodic symbolic sequencies correspond to periodic trajectories in phase space. So we have a complete knowledge of all localized orbits and in particular of all periodic orbits of the system (for more details, see [28]). Scattering trajectories running through the potential interior follow localized orbits for a finite time. Correspondingly, bundles of scattering trajectories can be labelled by finite binary symbolic sequences, according to the way in which they can be overshadowed by periodic orbits for a finite time. In the following we fix energy and incoming direction and consider the scattering angle as function of the impact parameter b. The bundle of stable manifolds of Λ intersects the b axis on a Cantor set. The deflection function is singular for initial conditions on stable manifolds of Λ, i.e. on points of this Cantor set. It is smooth in the gaps in between the points of the Cantor set. These gaps will therefore be called intervals of continuity. Also for this Cantor set and its gaps along the b axis we find a binary signature, we use the two symbols L (left) and R (right). The two intervals of the first generation are labelled by L and R. In generation N we find 2^N intervals and label them by symbol sequences of length N. To each interval of generation N there are two smaller neighbouring intervals of generation $N+1$. One of them lies on the left side and one of them on the right side of the corresponding parent interval of generation N. The signatures of

the new intervals are formed by attaching L (left) or R (right) to the signature of the parent interval. In this way the intervals of continuity form a binary branching tree along the b axis. For more details and some figures, see [15].

In [29] the effects of the chaos on the classical differential cross section are identified. In particular, the cross section contains an infinite number of rainbow singularities arranged in such a pattern, that their accumulation points form a fractal set which reflects the fractal structure of the localized chaotic set Λ in phase space.

In the present paper we construct the semiclassical scattering amplitude for system (1) by Maslov's version of the WKB method [30] which has been cast into a practical form for scattering systems in [31, 32]. Our results are twofold. First, we find that for scattering systems of an appropriate structure the WKB method works even in the chaotic case. This is an enormous difference to bound systems where this type of WKB construction is not possible for chaotic states. Second, we find properties of the cross section, which are not familiar from regular scattering systems and which therefore indicate classical chaos. In particular, the semiclassical cross section oscillates in a complicated pattern (related to classical fractal structures) in some regions of energy and angle, where the classical cross section is without significant structure.

In detail we proceed as follows. In section 2 we construct the classical Lagrangian submanifold $\mathcal{L}(\boldsymbol{p}_{\text{in}})$ corresponding to the asymptotic boundary condition of fixed incoming momentum $\boldsymbol{p}_{\text{in}}$. Section 3 contains the construction of the semiclassical scattering amplitude and cross section. In section 4 we observe how the classical rainbow singularities emerge in the semiclassical cross section in the limit of small $\hbar$. In section 5 we pull images of classical fractal structures out of the interference oscillations of the cross section. Section 6 contains discussions and a few remarks as to what extent the results of our model systems are typical for any chaotic scattering system.

2. The Lagrangian submanifold

The straight-line asymptotes of the system are labelled by the three quantities E, α, b. E is the energy; in the asymptotic region $E = (p_x^2 + p_y^2)/2$, where p_x, p_y are the momenta conjugate to x, y. α is the direction of the incoming momentum, $\alpha = \tan^{-1}(p_y/p_x)$. b is the impact parameter, $b = (xp_y - yp_x)/\sqrt{2E}$. The scattering angle θ is the difference between the directions of the outgoing and the incoming momentum. All angles are defined up to shifts by an integer multiple of 2π.

The first step in our procedure towards the semiclassical cross section is the construction of the classical Lagrangian submanifold $\mathcal{L}(\boldsymbol{p}_{\text{in}})$ belonging to the fixed incoming momentum $\boldsymbol{p}_{\text{in}}$. In position space we choose a straight line $\mathcal{G}$ perpendicular to $\boldsymbol{p}_{\text{in}}$ and far away from the origin such that along $\mathcal{G}$ the value of V cannot be distinguished from zero within the computational accuracy. $\mathcal{G}$ is placed on that side of the origin, from which it will be transported towards the potential by the flow. Along $\mathcal{G}$ the impact parameter b is taken as coordinate. The corresponding one-dimensional line $\bar{\mathcal{G}}$ in the four-dimensional phase space is obtained by lifting $\mathcal{G}$ to the constant momentum value $\boldsymbol{p}_{\text{in}}$. Next we transport $\bar{\mathcal{G}}$ through the phase space by the flow φ_t of the system. Thereby a two-dimensional submanifold $\mathcal{L}(\boldsymbol{p}_{\text{in}})$ is created. For the arbitrary point Q on $\mathcal{L}$ we take w and t as coordinates, where w is the impact parameter with which the trajectory through Q has started, i.e.

$$w(Q) = \lim_{t \to -\infty} b(\varphi_t(Q)) \tag{2}$$

and t is the time of flight for the trajectory starting in $(b, 0)$ on $\bar{\mathcal{G}}$ to arrive at Q. The surface $\mathcal{L}$ twists and turns in phase space and grows folds and whirls. By the time it has been transported through the potential interior it lies in an infinite number of branches over the position space.

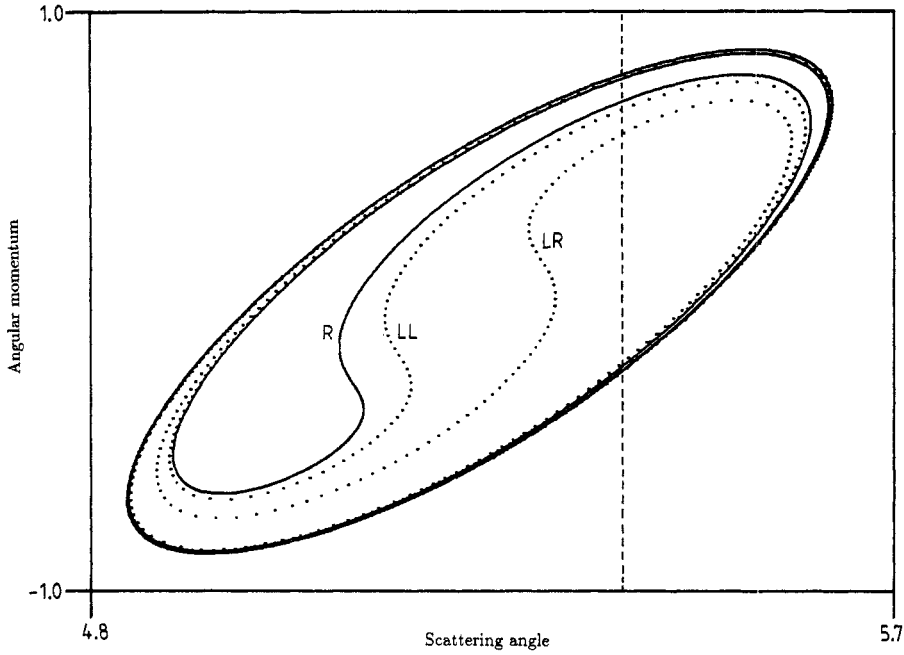

Figure 1. Intersection between the outgoing asymptotic plane and some branches of $\mathcal{L}(\boldsymbol{p}_{\mathrm{in}})$ for $\boldsymbol{p}_{\mathrm{in}} = (-\sqrt{1.2}, 0)$. The scattering angle value $\theta = 5.40$ is marked by a broken line.

For scattering systems we are mainly interested in the form of $\mathcal{L}$ in the outgoing asymptotic region. For a chaotic scattering system the mapping from points of $\bar{\mathcal{G}}$ into the outgoing asymptotes has discontinuities on a Cantor set along $\bar{\mathcal{G}}$. Each interval of continuity of b values in between the points of the Cantor set is turned into a spiral-shaped whirl during the transport through the potential interior by the flow. Figure 1 shows the intersection of the trajectories starting in three intervals of continuity of the b axis (R, LR, LL in the notation of [15]) with the θ/L plane of outgoing asymptotes. θ is the scattering angle and L is the outgoing angular momentum; $\boldsymbol{p}_{\mathrm{in}} = (-\sqrt{1.2}, 0)$ has been chosen (this gives an energy value of $E = 0.6$). The other intervals of continuity give similar spirals all converging towards the same boundary line. The set of all these spirals defines a fractal pattern whose accumulation points coincide with the unstable manifolds of Λ (see [29]).

In addition to the infinite number of spirals there is one further isolated branch of $\mathcal{L}(\boldsymbol{p}_{\mathrm{in}})$ coming from trajectories with large values of b which pass the potential hills on the outside instead of running through the potential interior. The outgoing angular momentum L of these trajectories is approximately $L \approx 2.5$ for the angle region shown in figure 1. Therefore this branch is outside the frame of figure 1.

Later we need the trajectories starting on $\bar{\mathcal{G}}$ and going to a specific outgoing direction $\bar{\theta}$. As an example, the line $\bar{\theta} = 5.4$ is marked by a broken line in figure 1. The intersection between $\mathcal{L}$ and the line $\theta = \bar{\theta}$ will be denoted by $D(\bar{\theta})$. Each interval

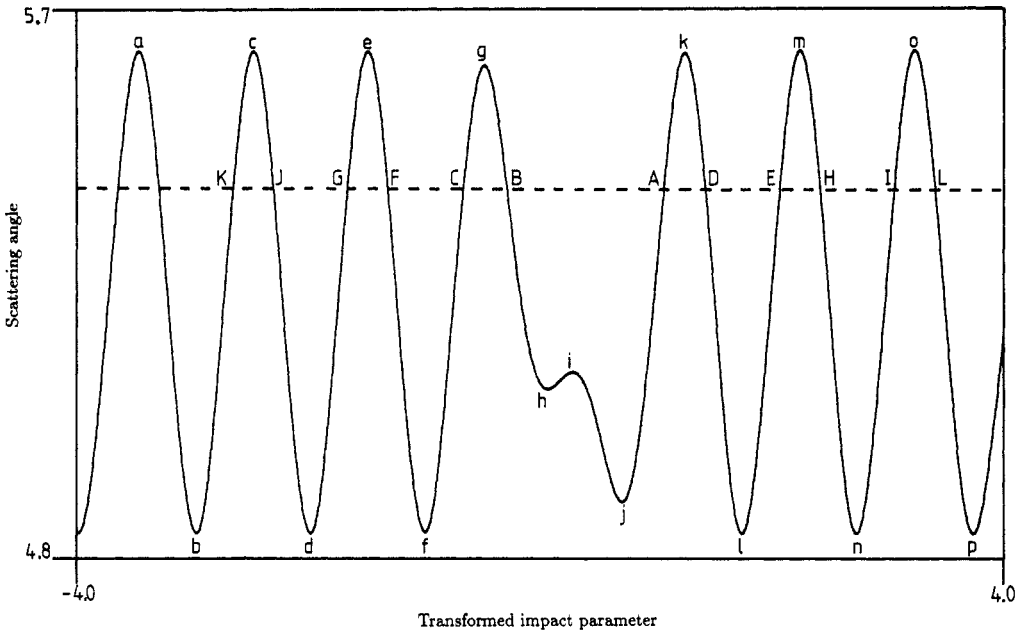

Figure 2. The deflection function $\theta(B)$ for interval R in logarithmically transformed coordinates according to equation (3). The contributions for $\theta = 5.40$ are labelled by capital letters. The extremal values are labelled by lower case letters.

of continuity contributes an infinite number of points to $D(\bar{\theta})$ as long as $\bar{\theta}$ is chosen such that the line $\theta = \bar{\theta}$ intersects the set of spirals at all. In this case $D(\bar{\theta})$ is a fractal set as has been explained in more detail in [29].

The knowledge of the deflection function $\theta(b)$ for an interval of continuity helps to correlate the spirals in figure 1 to values of the impact parameter. If we plot θ as a function of b itself, then the behaviour near the boundaries of the interval is not well resolved. Therefore we prefer to use the logarithmically transformed impact parameter

$$B(b) = \ln[(b - b_-)/(b_+ - b)]/\ln(\mu) \tag{3}$$

where b_- and b_+ are the boundaries of the interval under consideration. μ is the eigenvalue of the unstable periodic orbit oscillating on the saddle [15, 29]. Figure 2 displays $\theta(B)$ for the example of interval R. Also here the line $\theta = 5.4$ is marked by a broken line. For later reference some distinct points in figure 2 are labelled. Relative extrema, leading to rainbows in the cross section, are labelled by lower case letters. Intersections between the curve $\theta(B)$ and the line $\theta = 5.4$ are labelled by capital letters. Other intervals give very similar curves for $\theta(B)$ and a corresponding set of distinct points [29].

$\mathcal{L}(\boldsymbol{p}_{\text{in}})$ is Lagrangian. Therefore a global action function S exists on $\mathcal{L}$. We define

$$S(w,t) = \int p_x \mathrm{d}x + p_y \mathrm{d}y = \int \boldsymbol{p} \cdot \mathrm{d}\boldsymbol{q}. \tag{4}$$

The line integral is taken along a trajectory from $(b,0)$ to (w,t). We are dealing with a scattering problem, where the initial point $(b,0)$ and the final point (w,t) are supposed

to tend to infinity in position space and we wish to split off the uninteresting radial motion in the asymptotic region. Accordingly, we define a reduced action $\tilde{S}$ in which the asymptotic parts are split off:

$$\tilde{S}(w,t) = S(w,t) - \boldsymbol{p}\cdot\boldsymbol{q}|_{\text{final}} + \boldsymbol{p}\cdot\boldsymbol{q}|_{\text{initial}} = -\int \boldsymbol{q}\cdot \mathrm{d}\boldsymbol{p}. \tag{5}$$

$\tilde{S}$ has a definite value for each scattering trajectory independent of the choice of the initial and final point along this trajectory as long as these points are both far away from the potential region. $\tilde{S}$ gives the phase of the contribution of this trajectory to the semiclassical scattering amplitude [33]. In polar coordinates r, φ and their conjugate momenta p_r, L we find

$$\tilde{S}(w,t) = -\int r\,\mathrm{d}p_r + \int L\,\mathrm{d}\varphi. \tag{6}$$

3. Construction of the cross section

In the first part of this section we give a very brief description of the construction of the semiclassical wavefunction and scattering amplitude. The method is presented in full detail in [30–32]. On $\mathcal{L}(\boldsymbol{p}_{\text{in}})$ we define a density

$$\rho(w,t) = \rho_{\text{in}}(b)/J(w,t) \tag{7}$$

with

$$J(w,t) = \det \frac{\partial q(w,t)}{\partial(w,t)}$$

where $q(w,t)$ is the position space point onto which (w,t) projects. $\rho_{\text{in}}(b)$ is an incoming density on $\mathcal{G}$ which is supposed to be constant for our boundary conditions. On each open subset of $\mathcal{L}(\boldsymbol{p}_{\text{in}})$, which projects one-to-one onto the position space we construct the wavefunction

$$\chi(w,t) = \rho(w,t)^{1/2}\exp[\mathrm{i}S(w,t)/\hbar - \mathrm{i}\pi\mu/2] \tag{8}$$

where μ is the Maslov index of the trajectory from $(b,0)$ to (w,t). In our system it coincides with the number of caustics of $\mathcal{L}(\boldsymbol{p}_{\text{in}})$ crossed by this trajectory. In general $\mathcal{L}$ lies in many sheets over the position space and the semiclassical Schrödinger wavefunction $\psi(x,y)$ in configuration space is obtained by summation of χ over all the branches of $\mathcal{L}$ lying over (x,y), i.e.

$$\psi(x,y) = \sum_j \rho_j(w_j,t_j)^{1/2}\exp[\mathrm{i}S_j(w_j,t_j)/\hbar - \mathrm{i}\pi\mu_j/2] \tag{9}$$

where (w_j,t_j) projects onto (x,y) for all j.

Along caustics $\mathcal{L}$ does not project one-to-one onto the position space and the the density ρ in equation (7) diverges. Therefore the form of the wavefunction in equations (8) and (9) is not a useful semiclassical approximation. Near caustics $\mathcal{L}$

projects one-to-one onto the momentum space and we can construct an approximation to the momentum space wavefunction in terms of exp functions. Then we Fourier transform this non-singular momentum space wavefunction in order to obtain a non-singular position space wavefunction. By a smooth monotonic transformation of the integration variable the Fourier integral can be transformed into an appropriate normal form. It is the integral over a product of a slowly varying amplitude function times the exp function of a polynomial. If the caustic is an isolated fold of $\mathcal{L}$, then we need a polynomial of order three and the integral gives a combination of an Airy function and its derivative. If the caustic is a cusp or two neighbouring folds which are not well separated, then we need a polynomial of order four and the integral gives a combination of a Pearcy function and its derivatives. More complicated caustics do not occur in system (1).

The Airy and Pearcy contributions from the surroundings of caustics have to be joined smoothly to the exp functions from regions far away from caustics. This is done by appropriate partitions of unity on $\mathcal{L}$. The theory of this switching between position and momentum space is presented in mathematically rigorous form in [30]. More detailed explanations of the explicit construction of singularity-free semiclassical wavefunctions can be found in [31, 32, 34–36].

In the outgoing asymptotic region we separate the function (9) into a radial and an angular part. ρ splits as

$$\rho = r^{-1}\left|\frac{\mathrm{d}\theta}{\mathrm{d}b}(b_j)\right|^{-1}$$

and from S we add the asymptotic radial contributions $\boldsymbol{q}_{\mathrm{in}}\cdot\boldsymbol{p}_{\mathrm{in}}$ and subtract $\boldsymbol{q}_{\mathrm{out}}\cdot\boldsymbol{p}_{\mathrm{out}}$ giving $\tilde{S}$, already introduced in equation (5). For the signs in (5) note that $\boldsymbol{q}_{\mathrm{in}}$ and $\boldsymbol{p}_{\mathrm{in}}$ point in opposite directions whereas $\boldsymbol{q}_{\mathrm{out}}$ and $\boldsymbol{p}_{\mathrm{out}}$ point in the same direction. In the limit $r\to\infty$ we have $-\boldsymbol{q}_{\mathrm{in}}\cdot\boldsymbol{p}_{\mathrm{in}} = r_{\mathrm{in}}k$ and $\boldsymbol{q}_{\mathrm{out}}\cdot\boldsymbol{p}_{\mathrm{out}} = r_{\mathrm{out}}k$ where $k=\sqrt{2E}$. So we can split off the same radial factor $r^{-1/2}\exp[\mathrm{i}k(r_{\mathrm{in}}+r_{\mathrm{out}})]$ from each term in (9). The remaining angular factor of the wavefunction in the outgoing asymptotic region is just the semiclassical scattering amplitude. We obtain the well known expression [33]

$$f(\theta) = \sum_j \sqrt{c_j}\exp[\mathrm{i}\tilde{S}_j(\theta)/\hbar - \mathrm{i}\pi\mu_j/2] = \sum_j d_j \tag{10}$$

where

$$c_j = \left|\frac{d\theta}{db}(b_j)\right|^{-1}$$

is the contribution of trajectory j to the classical cross section. The sum runs over all classical trajectories starting with incoming momentum $\boldsymbol{p}_{\mathrm{in}}$ and going out with scattering angle θ. Also in (10) we need an uniformization close to caustics. It is induced by the uniformization of the wavefunction. The differential cross section is given by

$$\frac{\mathrm{d}\sigma}{\mathrm{d}\theta}(\theta) = |f(\theta)|^2.$$

For system (1) the sum in (10) converges absolutely as long as E is not too close to E_S. First consider the sum over the contributions from one particular interval of continuity, e.g. interval R shown in figure 2. For any particular value of the angle θ we group these contributions into four classes. For the example of $\theta = 5.4$ shown in figure 2 by a broken line, class 1 contains the points B, F, J, etc; class 2 contains C, G, K, etc; class 3 contains A, E, I, etc; class 4 contains D,H,L, etc. Any class contains a sequence of second-next-neighbouring points running towards one boundary of the interval and leading to a given value of θ. Going from one contribution of any class to the next one of the same class, the weight $\sqrt{c_j}$ of the contribution decreases by a factor $\sqrt{\mu}$ in the limit of close approach to the boundary [29]. μ, the larger eigenvalue of the saddle trajectory, is always greater than 1 since the saddle trajectory is unstable. For $E = 0.6$ we find $\mu \approx 107$, i.e.

$$c_{k+1,l} \approx c_{k,l}/\mu \tag{11}$$

where $c_{k,l}$ is the classical weight of the kth member of class l. For the sum of all contributions from interval R we find an estimate by a geometrical series

$$|f_R| \leq \sum_{l=1}^{4}\sum_{k=0}^{\infty}\sqrt{c_{k,l}} \approx \sum_{l=1}^{4}\sqrt{c_{0,l}}\sum_{k=0}^{\infty}\mu^{-k/2}. \tag{12}$$

Next we have to estimate the sum over all intervals. All intervals give similar sequences of contributions, the only difference being that the corresponding weights c_j are scaled proportional to the total length of the interval [29]. Let us group the intervals into various generations where the generation number is given by the length of the signature of the intervals introduced in [15]. There are 2^N intervals of generation N and each interval of generation N has two neighbouring intervals of generation $N+1$, whose signatures are obtained by adding either R or L to the signature of the parent interval. The ratio of the length of any interval compared to the length of its parent interval is always between $\mu^{-1/2}$ and $|\nu|^{-1/3}$, where ν is the eigenvalue of the unstable periodic ring trajectory. For $E = 0.6$ we find $\nu = -83$. In [28] this scaling behaviour is explained in detail and a plot of μ and ν as function of E is shown there. In our system we find $\mu^{-1/2} < |\nu|^{-1/3} < 1$ for any $E \in [E_S, E_M]$. This means, the weights $\sqrt{c_j}$ of the contributions of any interval to sum (10) are decreased by a factor of at least $|\nu|^{-1/6}$ compared to the corresponding weights $\sqrt{c_j}$ of the parent interval. Let n be an index which numbers the 2^N intervals of generation N and let $f_{n,N}$ be the contribution of interval n of generation N to sum (10). According to what has been explained above, we find

$$|f_{n,N}| \leq |\nu|^{-N/6}|f_{1,1}| \tag{13}$$

for any $n \in \{1, ..., 2^N\}$ and any $N > 1$. For the total amplitude we have the estimate

$$|f| \leq \sum_{N=1}^{\infty}\sum_{n=1}^{2^N}|f_{n,N}| \leq \sum_{N=1}^{\infty}2^N|\nu|^{-N/6}|f_{1,1}|. \tag{14}$$

This sum converges, if $|\nu| > 2^6 = 64$ which is fulfilled for $E > 0.58$. Then the sum over all intervals can be estimated by a converging geometric series.

The estimates used in (13) and (14) are very rough since we have always inserted the greatest scaling factors which can occur at all. A more careful estimate using the average scaling factor instead of $|\nu|^{-1/6}$ indicates that we may expect to find absolute convergence for energies as low as 0.52. However, for energies close to E_S there is definitely no absolute convergence of the semiclassical sum (10).

Also for most other chaotic scattering systems we expect energy intervals to exist, in which the semiclassical sum is not absolutely convergent. In these cases an appropriate resummation has to be applied which might be constructed along the pattern of rearrangement of the semiclassical series mentioned in [27].

In case of absolute convergence we can set a limit of accuracy and take only a finite number of branches of $\mathcal{L}(p_{in})$ into account which are needed in order to stay within the given limit of accuracy. In this paper we are mainly interested in demonstrating the method and in qualitative results. For this purpose it is sufficient to take the following branches of $\mathcal{L}(p_{in})$, which give the most important contributions for angle values around $\theta = 5\pi/3$: From each of the intervals R, LR, LL, RLL we take the nine most important branches respectively. In addition we take the isolated branch from trajectories not entering the potential interior. This branch gives the strongest contribution of all. In the following we shall call the contribution from this outer branch the background.

Of course, the correct asymptotic boundary condition for a scattering system is a constant density on the incoming impact parameter line. Nevertheless, it is informative to know in addition the contribution to the cross section coming from one particular interval of continuity along the b axis. This corresponds to a density ρ_{in} which is zero outside this one particular interval and constant inside. Therefore, besides showing the complete cross section containing the contributions from the four intervals mentioned above and the background, we present figures of the cross section coming from one interval. Note: the complete cross section is not the sum of the cross sections from the various intervals; in addition it contains interference terms.

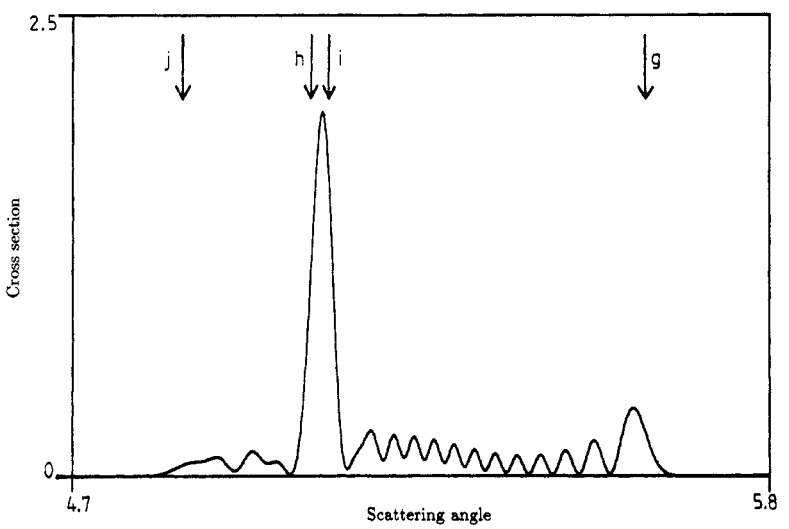

Figure 3. Contribution of interval R to the cross section for $\hbar = 0.005$ and $p_{in} = (-\sqrt{1.2}, 0)$. The positions of the most important classical rainbows are marked by arrows.

Figure 3 gives the cross section from interval R for $\hbar = 0.005$ in the angle range $\theta \in [4.7, 5.8]$. We took those nine branches from interval R with the highest weights to sum up $f_R(\theta)$ and plotted $|f_R(\theta)|^2$. Around $\theta = 5.6$ we see a strong contribution from the rainbow labelled g in figure 2. The other rainbows at neighbouring angle values (e and k, etc in figure 2) give quite weak contributions only and do not modify the curve significantly. The position of rainbow g is marked by an arrow in figure 3. Between $\theta = 5.08$ and $\theta = 5.106$ we see the strong contribution from the double rainbow labelled h and i in figure 2. Also their positions are marked by arrows. For $\hbar = 0.005$ these two rainbows are not well separated and we have used a Pearcy function for the uniformization of their contribution to the amplitude. Around $\theta = 4.9$ we find a destructive interference between the contributions from the rainbows labelled j and f in figure 2. The position of rainbow j is marked by an arrow in figure 3.

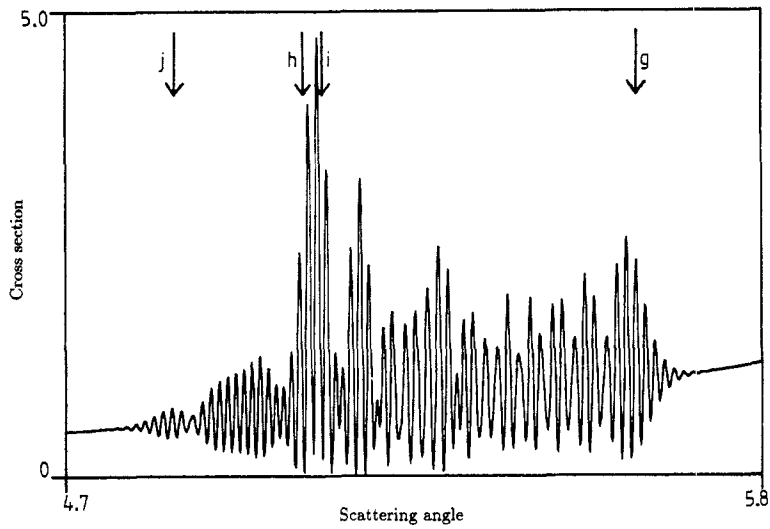

Figure 4. Complete cross section for $\hbar = 0.005$ and $p_{in} = (-\sqrt{1.2}, 0)$.

All other intervals give qualitatively similar cross sections, only with less weight according to their length on the b axis and with the positions of the rainbows shifted. For the double rainbow from the middle of the interval this shift can be appreciable (see also figure 10 in [29]). For the other rainbows the shift is quite small (compare the spirals in figure 1). Figure 4 shows the complete cross section in the angle interval $[4.7, 5.8]$, again for $\hbar = 0.005$. It includes the contributions from the intervals R, LR, LL, RLL and the background. The interference with the background causes the fast oscillations. An interesting property of $d\sigma/d\theta$ is the destructive interference between the caustic contributions near $\theta = 4.9$. For $\hbar = 0.005$ the various caustic contributions are not well separated along the θ axis and we have many overlapping rainbow structures. This causes an effect which reminds us of the anticaustic effect (decreased amplitude of the wavefunction at the position of clusters of caustics) mentioned in [37]. The arrows in figure 4 coincide with those in figure 3.

For comparison, figure 5 shows the corresponding classical cross section for which we have taken into account exactly the same branches of $\mathcal{L}$ that we have taken for the semiclassical cross section in figure 4. The four most important rainbows from interval R are labelled by lower case letters corresponding to the labels of the extrema

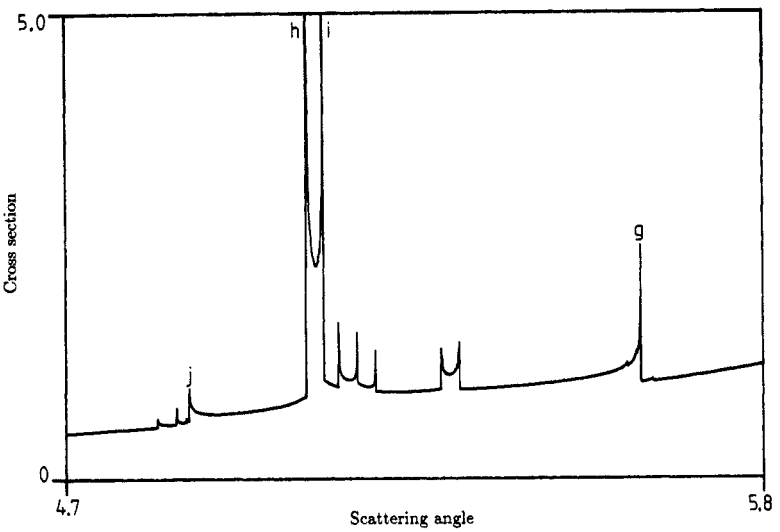

Figure 5. Classical cross section for $p_{in} = (-\sqrt{1.2}, 0)$. The four most important rainbows coming out of interval R are labelled by lower case letters corresponding to the labels of the deflection function in figure 2.

of the deflection function in figure 2. The comparison makes evident that at $\hbar = 0.005$ the various classical rainbows are not well resolved in the semiclassical cross section. We have to go to smaller values of $\hbar$ in order to see the classical rainbows growing out of the semiclassical cross section. This will be done in the next section. Close to the side boundaries of figures 4 and 5, i.e. for angle values close to 4.7 or 5.8, there is only a contribution from one branch of $\mathcal{L}$ (the background). Accordingly there are no interference oscillations in the semiclassical cross section and it coincides with the classical cross section.

4. Emergence of rainbows for small $\hbar$

The most prominent feature of chaos in the classical cross section is a fractal arrangement of rainbow singularities. In this section we investigate how the classical rainbows grow out of the semiclassical cross section in the limit of small $\hbar$.

In figure 6 we take the angle interval [4.86, 4.91], set $\hbar = 10^{-4}$ and plot the contribution of interval R to the cross section. For this value of $\hbar$ the rainbow labelled by j in figure 2 and marked by an arrow in figure 3 is clearly separated from the other rainbows of interval R (f, l, etc in figure 2). The corresponding plot for the contribution from interval LR (the next important one) is shown in figure 7. Also here the position of a classical rainbow (the one which corresponds to j for interval R) is marked by an arrow. Figure 8 shows the complete cross section in this angular interval for $\hbar = 10^{-4}$. The two arrows in figure 8 correspond to those in figures 6 and 7. Again the fast oscillations come from the interference with the background. In contrast to the situation for $\hbar = 0.005$ shown in figure 4, now for $\hbar = 10^{-4}$ the two rainbows j from intervals R and LR can be separated and identified individually in the complete cross section.

Also the shape of the contribution of the double singularity from the middle of interval R changes drastically during the transition from $\hbar = 0.005$ to $\hbar = 10^{-4}$ as

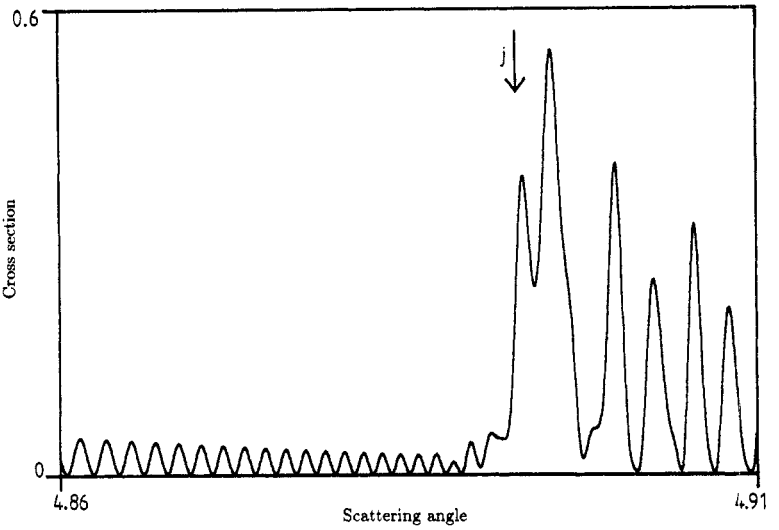

Figure 6. Contribution of interval R to the cross section for $\hbar = 0.0001$ and $p_{in} = (-\sqrt{1.2}, 0)$. The position of the most important classical rainbow is marked by an arrow.

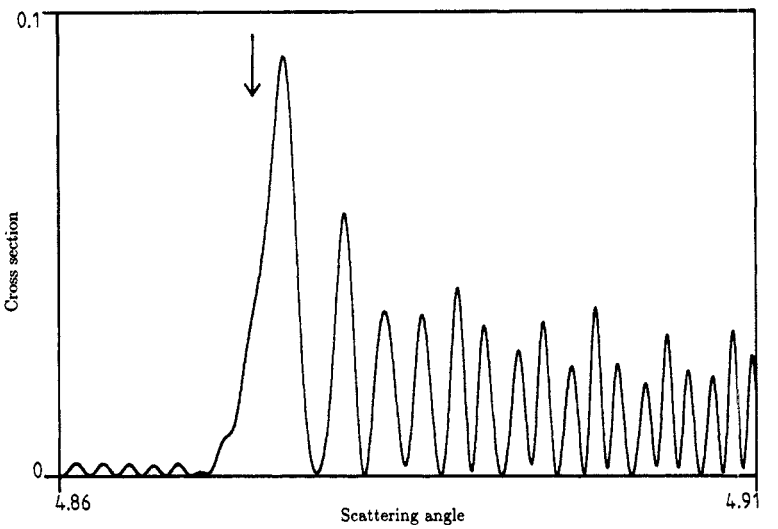

Figure 7. Contribution of interval LR to the cross section for $\hbar = 0.0001$ and $p_{in} = (-\sqrt{1.2}, 0)$. The position of the most important classical rainbow is marked by an arrow.

can be seen from figures 9 and 10. Figure 9 displays the contribution from interval R in the angle range [5.07, 5.12] for $\hbar = 10^{-4}$. The rainbows h and i (marked by arrows) are clearly separated in this case and their contributions to the amplitude can be described by two Airy functions. When we decrease $\hbar$ further, then these two rainbows behave like two well separated rainbows independent of each other. Figure 10 gives the complete cross section for $\theta \in [5.07, 5.12]$ and $\hbar = 10^{-4}$. Also in the complete cross section the rainbows h and i can be identified clearly.

For figures 11 and 12, $\hbar$ is decreased by a further factor of 100. Figure 11 gives

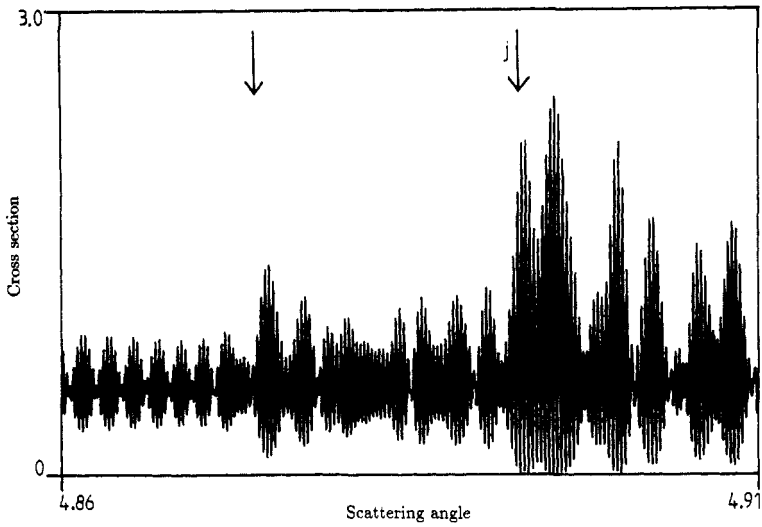

Figure 8. Complete cross section for $\hbar = 0.0001$ and $p_{in} = (-\sqrt{1.2}, 0)$. The arrows coincide with those in figures 6 and 7.

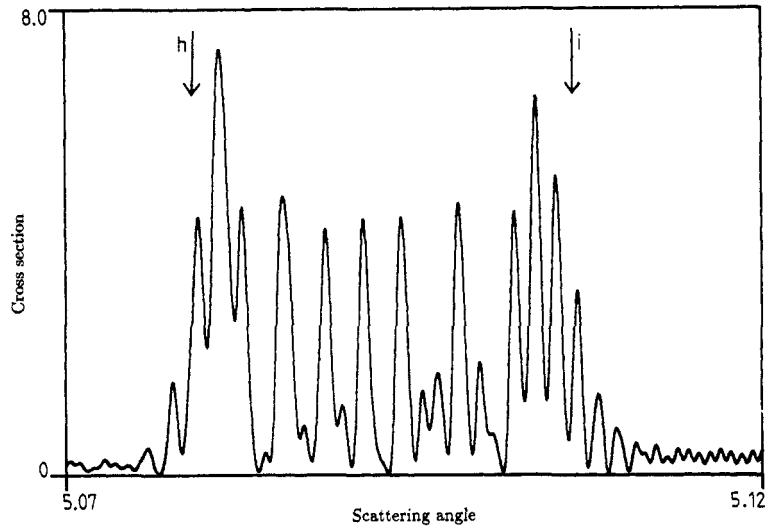

Figure 9. Contribution of interval R to the cross section for $\hbar = 0.0001$ and $p_{in} = (-\sqrt{1.2}, 0)$. The position of the most important classical rainbows is marked by arrows.

the cross section of R in the angular interval [4.8925, 4.894] for $\hbar = 10^{-6}$. Figure 12 shows the corresponding complete cross section. These figures show the same rainbow j (again marked by an arrow) as in figures 6 and 8. In figure 12 the fast interference oscillations with the background are not resolved. However, they are of the same qualitative structure as before, only compressed proportionally to the value of $\hbar$. The envelope curve of the rainbow structure clearly reminds us of a classical rainbow at $\theta = \theta_R$ with a shape like $(\theta - \theta_R)^{-1/2}$ on the illuminated side.

In the limit of small $\hbar$ the semiclassical cross section reproduces the classical cross section in the following way. The semiclassical cross section contains fast interference

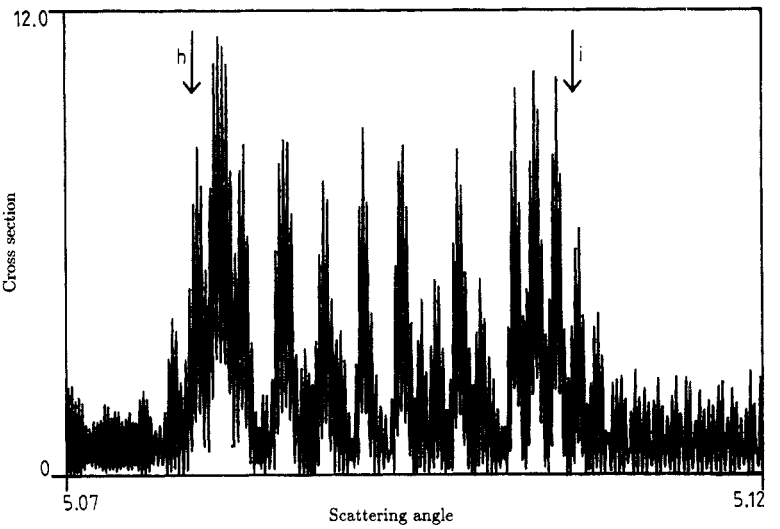

Figure 10. Complete cross section for $\hbar = 0.0001$ and $\boldsymbol{p}_{\text{in}} = (-\sqrt{1.2}, 0)$. The arrows coincide with those in figure 9.

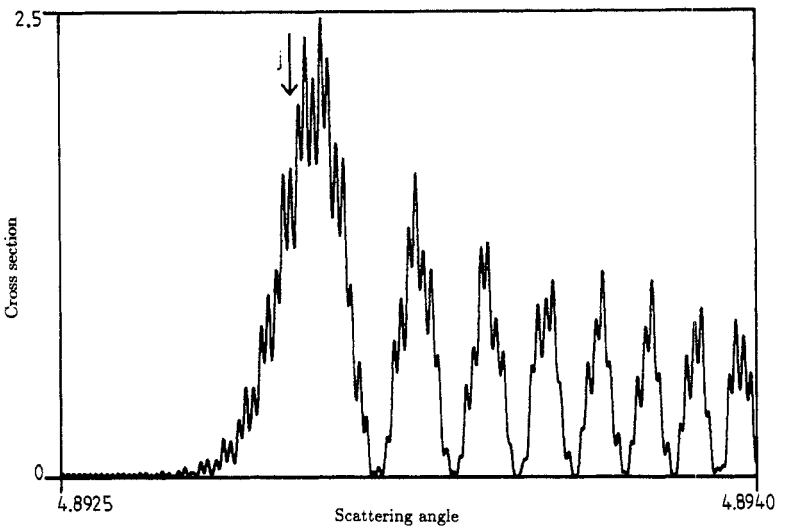

Figure 11. Contribution of interval R to the cross section for $\hbar = 10^{-6}$ and $\boldsymbol{p}_{\text{in}} = (-\sqrt{1.2}, 0)$. The position of the most important classical rainbow is marked by an arrow.

oscillations between the exp function contributions from the various well separated branches of $\mathcal{L}$. The length of these oscillations along the θ axis scales like $\hbar$. In addition, close to caustics there exist oscillations coming from the Airy function contributions. The width of the main peak of the Airy function is proportional to $\hbar^{2/3}$ and its height grows like $\hbar^{-1/3}$ in the limit of small $\hbar$. In our sequence of figures this scaling behaviour in $\hbar$ can be seen best in the figures showing the contributions from interval R only, e.g. in a comparison of rainbow j in figures 6 and 11. In this way sharp peaks of the cross section emerge in the limit of small $\hbar$ at the positions of the classical rainbows, which are located in a fractal arrangement. If we continue to

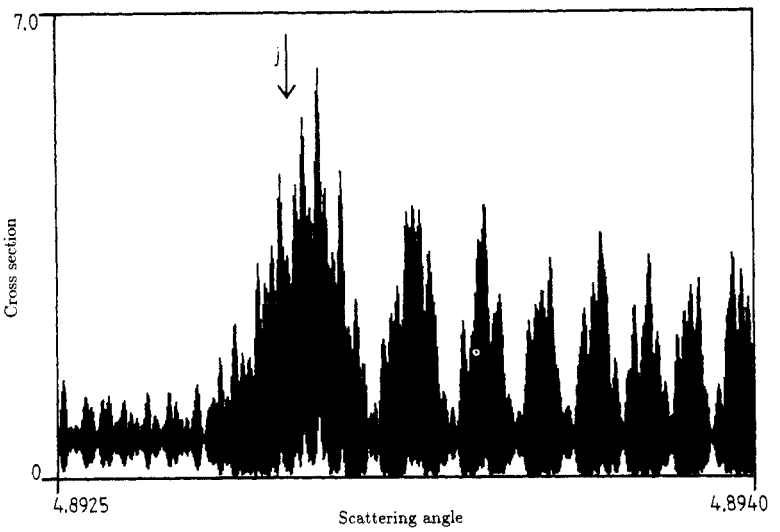

Figure 12. Complete cross section for $\hbar = 10^{-6}$ and $p_{\text{in}} = (-\sqrt{1.2}, 0)$.

decrease $\hbar$, then more and more smaller rainbows emerge and become well separated from neighbouring rainbows. To reproduce the classical cross section, let us average the semiclassical cross section for a particular value of $\hbar$ according to

$$\left\langle \frac{\mathrm{d}\sigma}{\mathrm{d}\theta}(\theta) \right\rangle = \frac{1}{2c} \int_{\theta-c}^{\theta+c} \frac{\mathrm{d}\sigma}{\mathrm{d}\theta}(\hat{\theta})\, \mathrm{d}\hat{\theta}.$$

We choose $2c$, the length of the averaging interval, proportional to $\hbar^{1/2}$ such that in the limit $\hbar \to 0$ the number of interference oscillations in the integration interval grows without limit. Also the width of the Airy peaks becomes small compared to the averaging length. When we let $\hbar$ tend to 0 in $\mathrm{d}\sigma/\mathrm{d}\theta$ and in c simultaneously, then $\langle \mathrm{d}\sigma/\mathrm{d}\theta \rangle$ approaches the classical cross section.

5. Fractal structures in the interference oscillations

Next we show how the semiclassical cross section contains information on classical fractal structures for values of E and θ far away from all classical rainbow singularities, i.e. in regions where the simple semiclassical approximation by exp functions is valid. The important quantity to be investigated is the local frequency spectrum of the interference oscillations in the cross section.

5.1. $\mathrm{d}\sigma/\mathrm{d}\theta$ as a function of E for fixed θ

In equation (10) we look at $\tilde{S}$ as a function of the energy E, keep θ fixed and expand $\tilde{S}(E)$ up to first order in E around a reference value E_0

$$\tilde{S}_j(E) = \tilde{S}_j(E_0) + (E - E_0) \left. \frac{\partial \tilde{S}_j}{\partial E} \right|_{E_0} + \mathrm{O}((E - E_0)^2) \tag{15}$$

where

$$T_j = \frac{\partial \tilde{S}_j}{\partial E}$$

is the time delay of trajectory j in the potential interior. Compared to $\tilde{S}(E)/\hbar$ the quantities $c_j(E)$ and $T_j(E)$ are slowly varying as functions of E in the limit of small $\hbar$ and they will be replaced by their value at E_0. With the abbreviation

$$\eta_j = -E_0 T_j(E_0)/\hbar + \tilde{S}_j(E_0)/\hbar - \pi\mu_j/2$$

the amplitude (10) becomes

$$f(E) = \sum_j \sqrt{c_j(E_0)} \exp(\mathrm{i}\eta_j) \exp(\mathrm{i}ET_j(E_0)/\hbar) \tag{16}$$

and the cross section is

$$\frac{\mathrm{d}\sigma}{\mathrm{d}\theta}(E) = |f(E)|^2 = \sum_j c_j + \sum_{j<k} \sqrt{c_j c_k}\ 2\cos[\eta_j - \eta_k + E(T_j - T_k)/\hbar]. \tag{17}$$

The first sum in (17) is the classical cross section. The second double sum represents the quantum mechanical interference terms. Their oscillation frequencies on the E axis are given by

$$\Omega_{j,k} = (T_j - T_k)/\hbar. \tag{18}$$

The set of accumulation points of the set of Ω values forms a fractal pattern.

To visualize this, we choose $\theta = 5.4$ and $E = 0.6$ and pick out from each interval of continuity the two trajectories corresponding to the points B and C in figure 2 for interval R. We plot $T_C - T_B$ for the various intervals in figure 13. The horizontal axis gives the time delay difference. The vertical axis gives the generation number of the intervals. In the bottom line we accumulate all time differences without sorting according to the generation. Some contributions are labelled with the signature of their interval. This plot has exactly the same structure as the fractal arrangement of rainbows given in figure 10 in [29]. Also the same analytical fit of the positions of the contributions can be taken over from equation (9) in [29]. Only the constants β and Δ in this equation acquire other numerical values. This structure reflects the arrangement of the unstable manifolds of the hyperbolic invariant set Λ in the classical phase space.

In the complete cross section in equation (17) there are not only interference terms between the contributions B and C within each interval. In addition, there are interferences between any two terms in the semiclassical amplitude sum (10). The set of all occurring differences of time delays is a very complicated fractal structure containing an infinite number of shifted copies of the structure shown in figure 13. We have therefore found a geometrical approach to characterize the complicated behaviour of $\mathrm{d}\sigma/\mathrm{d}\theta(E)$, somewhat complementary to the characterization by statistical properties given in [24–26].

Figure 14 is an example of $\mathrm{d}\sigma/\mathrm{d}\theta(E)$ for our model system, for $\hbar = 10^{-5}$ in part (*a*) and for $\hbar = 10^{-6}$ in part (*b*). The energy interval displayed is [0.6, 0.6005] and

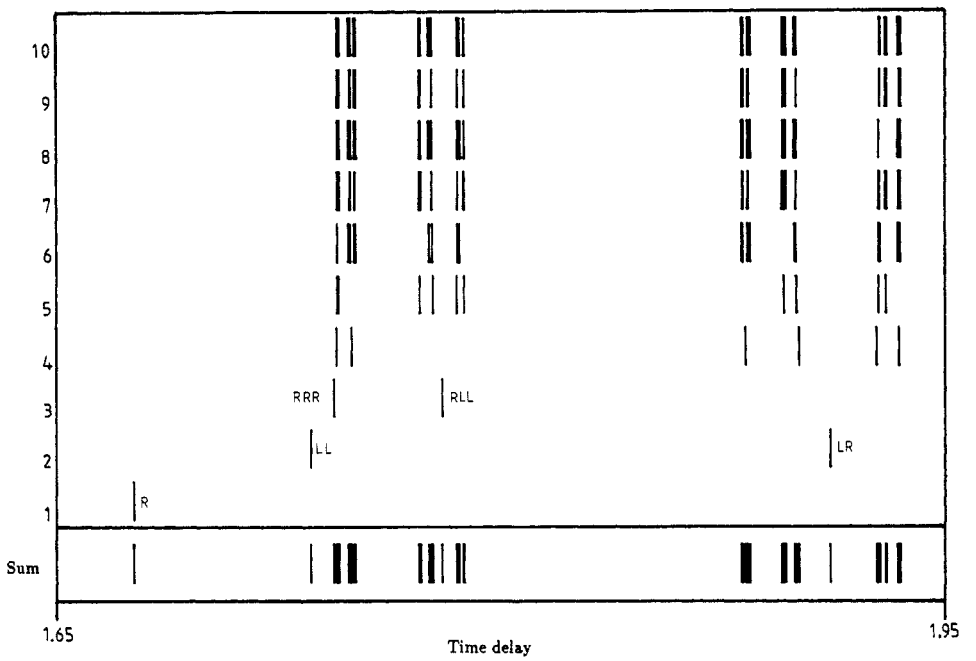

Figure 13. Difference of the time delays T_B and T_C for the intervals of generations 1–10. In the upper frame the contributions are sorted according to the generation number of the intervals. In the lower frame all contributions are accumulated.

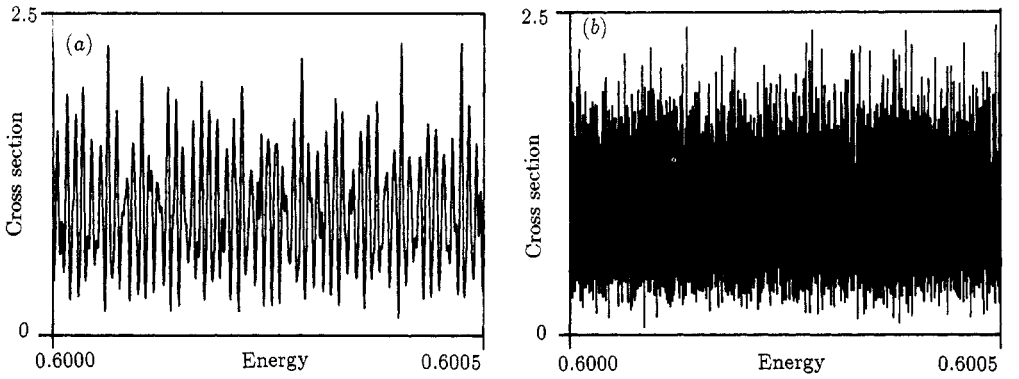

Figure 14. Cross section as function of the energy for fixed incoming direction $\alpha = \pi$ and fixed scattering angle $\theta = 5.40$, for (*a*) $\hbar = 10^{-5}$ and (*b*) $\hbar = 10^{-6}$.

$\theta = 5.4$ which is far away from all classical rainbows. We have taken into account the 32 most important branches of $\mathcal{L}(p_{\text{in}})$. Near $\theta = 5.4$ and $E = 0.6$ this leads to a relative error in the cross section of less than 0.04. In part (*b*) the fast oscillations are not well resolved. They are of the same qualitative structure as in part (*a*), only compressed by a factor ten. From the plot in part (*b*) we get an impression of the fluctuations on all scales which $\mathrm{d}\sigma/\mathrm{d}\theta(E)$ shows in the limit of small $\hbar$.

If the function $\mathrm{d}\sigma/\mathrm{d}\theta(E)$ is given inside an appropriate interval of values of E, then we can apply a local Fourier transformation to this function in order to recover an approximate picture of the distribution of time delays. For the resolution of this

procedure we can find estimates which are complete analogues to the ones given in [38] for the case of $d\sigma/d\theta$ as function of θ.

5.2. $d\sigma/d\theta$ as function of θ for fixed E.

We expand $\tilde{S}(\theta)$ up to first order in θ around some reference point θ_0:

$$\tilde{S}_j(\theta) = \tilde{S}(\theta_0) + (\theta - \theta_0)\left.\frac{\partial \tilde{S}_j}{\partial \theta}\right|_{\theta_0} + O((\theta - \theta_0)^2) \tag{19}$$

where $L_j = \partial \tilde{S}_j/\partial\theta$ is the outgoing angular momentum of trajectory j. With the abbreviation

$$\varphi_j = -\theta_0 L_j/\hbar + \tilde{S}_j(\theta_0)/\hbar - \pi\mu_j/2$$

we obtain

$$f(\theta) = \sum_j \sqrt{c_j}\exp(i\varphi_j)\exp(i\theta L_j/\hbar). \tag{20}$$

The frequencies in (20) are just the points of $D(\theta)$ which form a fractal set as we have seen in section 2. Therefore also the frequencies of the oscillations of the interference terms in the cross section

$$\frac{d\sigma}{d\theta}(\theta) = |f(E)|^2 = \sum_j c_j + \sum_{j<k}\sqrt{c_j c_k}\,2\cos[\varphi_j - \varphi_k + \theta(L_j - L_k)/\hbar] \tag{21}$$

form a fractal set. From a knowledge of the oscillation frequencies of the cross section the classical set $D(\theta_0)$ and finally $\mathcal{L}(\boldsymbol{p}_{in})$ in the asymptotic region can be reconstructed approximately. For more details on this possibility, some figures and a discussion of the limits of resolution, see [38].

6. Final remarks and conclusions

We have applied the WKB–Maslov method to a chaotic scattering system. This is possible because the semiclassical sum (10) converges absolutely in our case, despite of the infinite number of branches of $\mathcal{L}(\boldsymbol{p}_{in})$. A necessary condition for this convergence is the fact that in a scattering system most trajectories go off to infinity after a finite time and the number of trajectories which stay inside the potential interior longer than a given time T decreases exponentially with T. This is in sharp contrast to bound systems where most trajectories come back again and again giving an infinite number of contributions to the semiclassical sum. Therefore the WKB–Maslov method cannot be applied straight forewardly to a chaotic bound system. For bound systems an appropriate method of resummation has to be established first.

For our numerical examples we have considered the angle region around $\theta = 5\pi/3$ only. In the other two angle regions around $\theta = \pi$ and $\theta = \pi/3$, which are reached by trajectories leaving the potential interior through the other two saddles, the same structures of the cross section can be found. For other incoming directions nothing changes dramatically as long as there are trajectories entering the potential interior

at all, i.e. as long as the stable manifolds of Λ are intersected by the initial conditions p_{in} = fixed, b arbitrary (cf figure 9 in [15]).

For other values of E we see similar structures as long as E stays smaller than the maximal potential energy $E_M \approx 1.005$ and as long as E does not come too close to the saddle energy $E_S \approx 0.459$ where the semiclassical sum (10) is no longer absolutely convergent.

The most important intention of our work was to find some fingerprints of classical chaos in the semiclassical scattering cross section. The main results in this respect are the following. The scattering amplitude has fractal clusters of rainbows and shows oscillations on all scales in the limit of small $\hbar$. This is consistent with the predictions of the same properties for semiclassical chaotic wavefunctions given in [39]. We look at the system in the asymptotic range, where the radial degree of freedom is uninteresting and has been separated off. Therefore only one essential degree of freedom, the angle, remains. If we look at our construction from a more abstract point of view, we can characterize it like this. Given is a two-dimensional phase space with canonical coordinates θ and L and in it the Lagrangian submanifold $\mathcal{L}$, given by the spirals shown in figure 1. Along $\mathcal{L}$ the action function S and the Maslov index μ are given. We construct the wavefunction $f(\theta)$ for this Lagrangian submanifold according to the rules of Maslov. Of course, a structure like $\mathcal{L}(p_{in})$ shown in figure 1 could never be the Lagrangian submanifold for an autonomous system with one degree of freedom and a smooth Hamiltonian function. In those systems the invariant Lagrangian submanifolds—which are the curves H = constant—are homeomorphic to lines and/or circles but never to a fractal arrangement of spirals. However, in non-autonomous systems the Lagrangian submanifolds can grow infinite whirls and clusters of caustics, which come close to our spirals (see figures in [39]). Accordingly, in our scattering amplitude, which is constructed like a one-dimensional wavefunction to a non-autonomous system, we see phenomena of the type which have been observed in wavefunctions of one-dimensional non-autonomous systems.

By a careful study of the caustic positions and of the frequency spectra of the interference oscillations we can recover classical fractal sets out of the quantum cross section in the limit of small $\hbar$. Because $\hbar = 0$ is an essential singularity of quantum mechanics, we cannot take the value $\hbar = 0$ itself in an investigation of semiclassical quantities. We can only go to smaller and smaller values of $\hbar$ and see the images of classical fractal structures in quantum systems being resolved better and better on more and more levels of the infinite hierarchy of levels. But, it is not possible to have the classical fractals resolved on all infinite levels simultaneously.

System (1) is typical for chaotic scattering systems. Also in other chaotic scattering systems the topological chaos in phase space is caused by homoclinic and heteroclinic connections of unstable periodic trajectories running back and forth on saddles. Thereby a localized hyperbolic set is created; its stable and unstable manifolds reach out into the asymptotic regions and influence the scattering dynamics. The boundaries of the intervals of continuity on the impact parameter line are formed by the intersections of the stable manifolds of the saddle orbit. The image of the impact parameter line, which is created by the transport of the trajectories into the outgoing asymptotic θ/L plane, again consists of an infinite arrangement of whirled lines. Their accumulation points coincide with the unstable manifolds of the localized chaotic set. The scales of the fractal sets are essentially given by the eigenvalues of the most important (shortest) unstable periodic orbits. Thereby they are energy dependent. So far, in any more general chaotic scattering system everything goes as in our model system. The

difference is, that in general systems we do not know a complete and exact symbolic organization for the occurring fractal sets. Without a symbolic dynamics it is hard to sum up the semiclassical series in a systematic way and to give estimates on the accuracy obtained with a truncated sum. Except for these more technical problems we expect, that our results and conclusions are typical for any chaotic potential scattering system.

Acknowledgments

We thank Professor P H Richter for helpful remarks. This work has been supported financially by the Deutsche Forschungsgemeinschaft.

References

[1] Rankin C and Miller W H 1971 *J. Chem. Phys.* **55** 3150–6
[2] Gottdiener L 1975 *Mol. Phys.* **29** 1585-95
[3] Fitz D and Brumer P 1979 *J. Chem. Phys.* **70** 5527–5533
[4] Agmon N 1982 *J. Chem. Phys.* **76** 1309–16
[5] Schlier C 1983 *Chem. Phys.* **77** 267–5
[6] Noid D, Gray S and Rice S 1986 *J. Chem. Phys.* **84** 2429–52
[7] Skodje R and Davis M 1988 *J. Chem. Phys.* **88** 2429–56
[8] Tiyapan A and Jaffe C 1989 Classical atom–diatom scattering: self similarity, scaling laws and renormalization *Preprint* Department of Physics, West Virginia University
[9] Brumer P and Shapiro 1988 *Adv. Chem. Phys.* **70** 365–439
[10] Petit J and Henon M 1986 *Icarus* **66** 536–55
[11] Henon M 1988 *Physica* **33**D 132–56
[12] Eckhardt B and Aref H 1989*Phil. Trans. R Soc.* A **326** 655–96
[13] Campbell D, Peyrard M and Sodano P 1986 *Physica* D **19** 165–205
[14] Eckhardt B and Jung C 1986 *J. Phys. A: Math. Gen.* **19** L829–33
[15] Jung C and Scholz H-J 1987 *J. Phys. A: Math. Gen.* **20** 3607–17
[16] Jung C and Scholz H-J 1988 *J. Phys. A: Math. Gen.* **21** 2301–11
[17] Troll G and Smilansky U 1989 *Physica* D **35** 34–64
[18] Gaspard P and Rice S 1989 *J. Chem. Phys.* **90** 2225–41, 2242–54, 2255–62
[19] Eckhardt B 1988 *Physica* D **33** 89–98
[20] Smilansky U 1990 *Les Houches Session LII, Course X* ed M J Giannoni, A Voros and J Zinn-Justin (Amsterdam: Elsevier)
[21] Tel T 1989 *J. Phys. A: Math. Gen.* **22** L691–7
[22] Kovacz Z and Tel T 1990 *Phys. Rev. Lett.* **64** 1617–20
[23] Gutzwiller M 1983 *Physica* D **7** 341–55
[24] Blümel R and Smilansky U 1988 *Phys. Rev. Lett.* **60** 477–80
[25] Blümel R and Smilansky U 1989 *Physica* D **36** 111–36
[26] Blümel R and Smilansky U 1990 *Phys. Rev. Lett.* **64** 241–4
[27] Cvitanovic P and Eckhardt B 1989 *Phys. Rev. Lett.* **63** 823–6
[28] Jung C and Richter P H 1990 *J. Phys. A: Math. Gen.* **23** 2847–66
[29] Jung C and Pott S 1989 *J. Phys. A: Math. Gen.* **22** 2925–38
[30] Maslov V and Fedoriuk M 1981 *Semiclassical Approximation in Quantum Mechanics* (Dordrecht: Reidel)
[31] Delos J 1986 *Adv. Chem. Phys.* **65** 161–214
[32] Knudson S, Delos J and Bloom B 1985 *J. Chem. Phys.* **83** 5703–11
[33] Miller W H 1975 *Adv. Chem. Phys.* **30** 77–136
[34] Delos J 1987 *J. Chem. Phys.* **86** 425–39
[35] Connor J N L 1973 *Mol. Phys.* **26** 1217–31
[36] Connor J N L and Farrelly D 1981 *J. Chem. Phys.* **75** 2831–46
[37] Berry M V 1977 *J. Phys. A: Math. Gen.* **10** 2083–91
[38] Jung C 1990 *J. Phys. A: Math. Gen.* **23** 1217-24
[39] Berry M V and Balazs N L 1979 *J. Phys. A: Math. Gen.* **12** 625–42